Optimization of pulse-modulation based ToF imaging systems

Andreas Süss[†*], Yenn Leng Tan[‡], Maarten Rosmeulen[†], Bedrich J. Hosticka[*‡]

[*]Fraunhofer IMS, Finkenstrasse 61, 47057 Duisburg/Germany
[†]IMEC, Kapeldreef 75, B-3001 Leuven/Belgium
[‡]University Duisburg-Essen,
Tel: +32 16 281142, e-mail: andreas.suess.de@ieee.org

***Abstract*—This work is dedicated to efficient optimization of pulse-modulated (PM) indirect time-of-flight (iToF) through analytical modeling. Measurements that verify the validity of the model for two generations of CMOS iToF imagers are presented. As convexity is not guaranteed and e.g. eye-safety constraints have points of non-differentiability, the feasibility of Evolutionary Strategy (ES) optimizers was investigated. Compared to alternative non-differentiating global optimizers this has the advantage of offering systematic and random progress capability without the need for phenotype-genotype mapping. A MATLAB implementation is presented that demonstrates convergence of a problem with 6 degrees of freedom (DOF) in less than 100 iterations. Compared to the brute force approach this is an improvement by several orders of magnitude, as there computation time scales exponentially with the number of DOF.**

I. Introduction

From the beginning of this century CMOS based iToF imaging emerged as a popular research topic [1]–[7]. In a ToF setup an imager is employed to measure the time elapsing between emission and detection of a modulated light wave that is reflected by the scenery – typically in a diffusive manner - and focused onto the image sensor (Fig. 2). In order to achieve millimeter precision, high-speed photodetectors are necessary [1]–[7]. In the past, many publications focused on non-linearity of continuous-wave modulated (CW) ToF systems, on noise of CW and PM ToF systems [1], [7]–[9] and on the design of high-speed photodetectors [1]–[7]. It is widely accepted that ToF imaging is limited by photon noise. Also it was recently investigated that lower-speed photodetectors have impact on linearity in PM ToF systems [12]. For scenarios of low irradiance levels that are inherently difficult to measure accurately due to photon noise, another limitation occurs – the poor charge transfer at low irradiance levels due to less self-induced drift [5], [9]–[11]. This has impact on linearity as well as noise. Recently, the impact of these photodetector limitations amongst other limitations such as parasitic light sensitivity (PLS), saturation and circuit noise were thoroughly investigated [12]. Unfortunately, the numerical effort that method imposed was significant, resulting in the desire for more efficient approaches. The present work provides a model that relates photodetector imperfections, sensor timing and the optical setup in a simple but accurate way that allows for employment of efficient numerical optimization schemes such as evolutionary strategies (ES).

II. Analytical PM iToF Model

The optical setup (Fig. 2) can be modeled by geometrical optics [1], [7], [12]. Considering the PM TOF principle [5], [7], [12], [13], the emission of a light pulse is synchronized to a multitude of shutters (TX1-TX4) that are arranged such that fractions of the reflected light pulse are accumulated in a first (TX1) and second (TX2) shutter. Another shutter (TX3) is used as a reference of the ambient light level and a shutter (TX4) is employed to drain additional charge carriers (Fig. 2). A photodetector, such as a lateral drift-field photo detector (LDPD) [5], [12]–[14] is operated such that impinging charge carriers are propagated to the storage node of the corresponding activated shutter node very fast (Fig. 1).

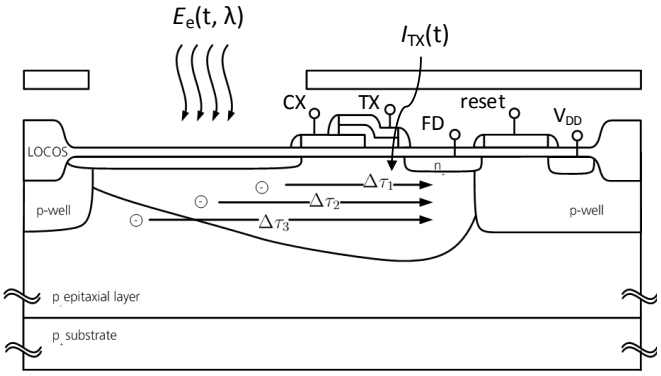

Figure 1. Cross sectional view of an LDPD [5], [12]–[14].

Assuming that all charge carriers are independent and have negligible effect on the potential profile of the detector, the current under the transfer gate I_{TX} can be expressed as a superposition of the charge carriers that are delayed depending on the distance they have to travel to the storage node $\Delta\tau_i$. The resulting expression takes the form of a convolution integral:

$$I(t) \propto \sum_i E_{\mathrm{e}}(t-\Delta\tau_i)\cdot h_i \approx \int_0^\infty E_{\mathrm{e}}(t-\tau)\cdot h(\tau)\mathrm{d}\tau. \quad (1)$$

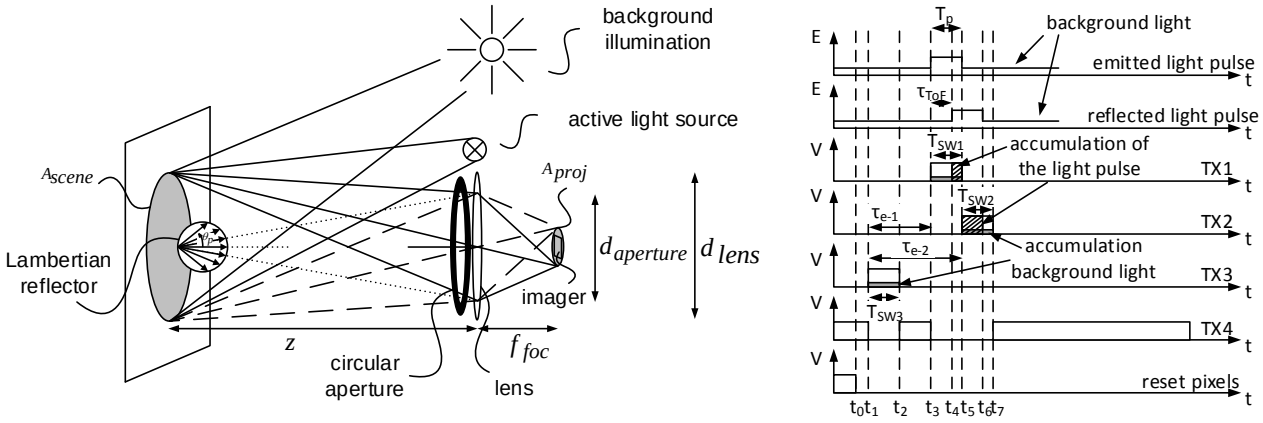

Figure 2. Simplified schematic of the range measurement setup (left) , basic MSI PM ToF timing (right) [12]

The obtained current is then integrated by the shutter operation. In addition, the shutter accumulates dark current I_{dark} as well as parasitically propagated charge carriers:

$$N_{\mathrm{e}^-} = N_{\mathrm{accu}} \cdot \eta_{\mathrm{ext}} \cdot A_{\mathrm{pix}} \cdot FF \frac{\lambda}{h_{\mathrm{P}} c} \int_0^{f_{\mathrm{rep}}^{-1}} I(t) \cdot S(E_{\mathrm{e}}, t) \mathrm{d}t + \frac{N_{\mathrm{accu}} I_{\mathrm{dark}}}{f_{\mathrm{rep}} q}. \quad (2)$$

Here, N_{accu} is the repetition count of the timing illustrated in Fig. 2. η_{ext} is the external quantum efficiency, $A_{\mathrm{pix}} \cdot FF$ corresponds to the photoactive area of a pixel, λ is the wavelength of the employed light source, c is the speed of light and h_{P} is Planck's constant, f_{rep} is the repetition rate of the active light source, q is the elementary charge and S is the shutter function. For simplicity one may assume a simple low-pass characteristic for the kernel h:

$$h = \begin{cases} \tau_{\mathrm{LDPD}}^{-1} \cdot \exp(-t \cdot \tau_{\mathrm{LDPD}}^{-1}) \text{ , for } t \geq 0 \\ 0 \text{ , for } t < 0 \end{cases} \quad (3)$$

and an ideal short-time integrator operation disturbed by PLS:

$$S = \begin{cases} 1 \text{ , for TX ON} \\ PLS \text{ , for TX OFF} \end{cases} \quad (4)$$

A good fit between this model and measurement results of the shutter response characteristics has been obtained (Fig. 3) [12]. The response time of the photodetector improves with increasing irradiance (Fig. 3, 4). This can be explained by an increased self-induced drift [5], [9]–[12]. Fig. 4 depicts measurements of τ_{LDPD} for varying irradiance yielded from fits such as illustrated in Fig. 3 [12]. It is shown that in the range from $3\,\mathrm{W/m^2}$ to $3\,\mathrm{kW/m^2}$ τ_{LDPD} can be approximated by a logarithmic function [12].

In Table I measurement data of two generations of CMOS PM iToF imagers are presented [5], [12]. The PLS is in the order of $1\,\%$ and is currently the most important parameter for precision improvement (c.f. Fig. 5). For the

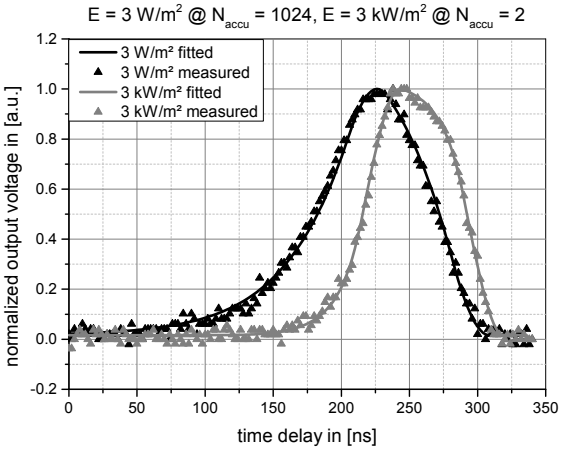

Figure 3. Measurements and model of LDPD pulse response [12].

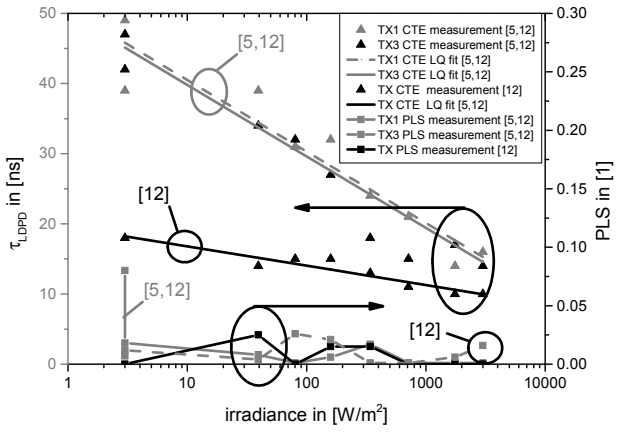

Figure 4. Measurements of LDPD charge transfer times and PLS as function of irradiance [12].

systematic error, however, it would be more important to improve the transfer time as this simplifies modeling of the relation between charge carrier count and depth information [12].

The presented simplified photodetector model combined with the optical setup and the sensor timing (Fig. 2) can now be used to compute the charge carrier count on the

Table I
MEASURED MODEL PARAMETERS OF DEVELOPED TOF PHOTODETECTORS [5], [12]

	gen. 1 [5], [12]	gen. 2 [12]
τ_{LDPD} @ $3\,\mathrm{kW/m^2}$	15 ns	10 ns
τ_{LDPD} @ $3\,\mathrm{W/m^2}$	45 ns	18 ns
Max. sensitivity mismatch @ $3\,\mathrm{kW/m^2}$	20 %	$< 0.1\,\%$
Max. sensitivity mismatch @ $3\,\mathrm{W/m^2}$	60 %	$< 0.1\,\%$
Nyquist frequency for $E_{\mathrm{e-amb}}$	$\frac{0.5}{t_{\mathrm{read}}+N_{\mathrm{accu}}\cdot T_{\mathrm{p}}/d} \approx 10\,\mathrm{Hz}$	$\frac{0.5}{T_{\mathrm{p}}/d} \approx 17\,\mathrm{kHz}$
dark current @ RT	$15\,000\,\mathrm{e^-/s}$	$6700\,\mathrm{e^-/s}$
$A_{\mathrm{pix}} \cdot FF$	$610\,\mu\mathrm{m}^2$	$190\,\mu\mathrm{m}^2$
PLS	1 %	1.5 %
ΔV_{out} @ LE $\leq 1\,\%$ (EMVA1288)	1.8 V	2 V
C_{SN}	12 fF	13 fF
FWC	$200\,\mathrm{ke^-}$	$240\,\mathrm{ke^-}$
CG	$9\,\mu\mathrm{V/e^-}$	$8.3\,\mu\mathrm{V/e^-}$

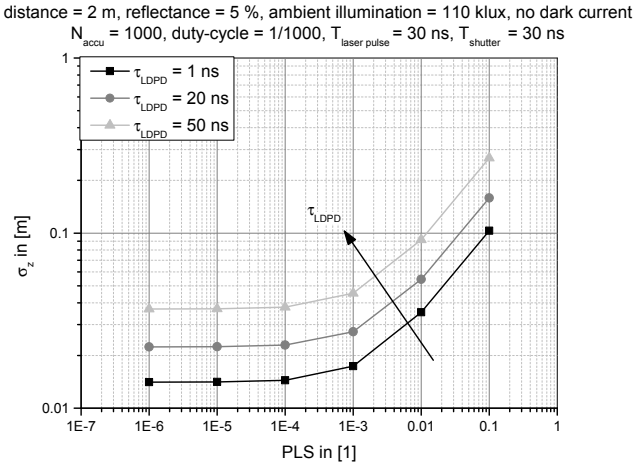

Figure 5. Impact of charge transfer time and PLS on depth precision [12].

storage node. To translate this to depth precision, Gaussian error analysis may be applied. Simulations show that the current systems are limited by CTE and PLS (Fig. 5). The inverse function that is needed for Gaussian error analysis cannot be analytically found from the presented model even though it is highly simplified [12]. A numerical regression of a multivariate polynomial function can be employed to find a power series expression of the inverse function, but results in large computation effort that makes this approach unattractive for optimization [12]. Alternatively, linearization can be employed to yield an analytical small-signal model that can be used for noise analysis. Therefore a linear map between variations of scenery parameters - depth z, reflectance r_{scene} and ambient light $E_{\mathrm{e-amb}}$ - and the charge carrier counts is defined:

$$\begin{pmatrix} \mathrm{d}\Delta N_1 \\ \mathrm{d}\Delta N_2 \\ \mathrm{d}N_3 \end{pmatrix} = \underbrace{\begin{pmatrix} \frac{\partial \Delta N_1}{\partial z} & \frac{\partial \Delta N_1}{\partial r_{\mathrm{scene}}} & \frac{\partial \Delta N_1}{\partial E_{\mathrm{e-amb}}} \\ \frac{\partial \Delta N_2}{\partial z} & \frac{\partial \Delta N_2}{\partial r_{\mathrm{scene}}} & \frac{\partial \Delta N_2}{\partial E_{\mathrm{e-amb}}} \\ \frac{\partial N_3}{\partial z} & \frac{\partial N_3}{\partial r_{\mathrm{scene}}} & \frac{\partial N_3}{\partial E_{\mathrm{e-amb}}} \end{pmatrix}}_{=J(z,r_{\mathrm{scene}},E_{\mathrm{e-amb}})} \cdot \begin{pmatrix} \mathrm{d}z \\ \mathrm{d}r_{\mathrm{scene}} \\ \mathrm{d}E_{\mathrm{e-amb}} \end{pmatrix} \quad (5)$$

Here, $\Delta N_i = N_i - N_3, i \in \{1, 2\}$ was used. Provided the Jacobian $J(z, r_{\mathrm{scene}}, E_{\mathrm{e-amb}})$ is not singular an inverse can be found, which can subsequently be used to obtain the depth precision

$$\sigma_z^2 = \frac{1}{\det^2(J)} \cdot \left[\left| \frac{\partial \Delta N_2}{\partial r_{\mathrm{scene}}} \cdot \frac{\partial N_3}{\partial E_{\mathrm{e-amb}}} \right|^2 \sigma_{\Delta N_1}^2 + \left| \frac{\partial \Delta N_1}{\partial r_{\mathrm{scene}}} \cdot \frac{\partial N_3}{\partial E_{\mathrm{e-amb}}} \right|^2 \sigma_{\Delta N_2}^2 \right]. \quad (6)$$

Here, $\partial \Delta N_i / \partial E_{\mathrm{e-amb}} = 0$ was used. The uncertainty of the charge carrier counts can be computed by standard models for photon noise, dark current shot noise, reset noise and noise of the readout chain (c.f. [12]).

III. ES OPTIMIZATION

For optimization a figure of merit (FOM) needs to be defined that guarantees functionality over the entire dynamic range – here, defined by depth range, reflectance range and desired tolerable ambient light. For simplicity a numerical approximation of an integrating measure is chosen

$$FOM = \sum_i \sum_j \sum_k \omega_{ijk} \sigma_z^2(z, r_{\mathrm{scene}}, E_{\mathrm{e-amb}}). \quad (7)$$

The weights ω can be tuned to put emphasis on scenarios that might be more important for a certain application. For this work, however, they were set to 1.

As the IEC eye-safety regulations have points of non-differentiability, a direct approach of solving the Karush-Kuhn-Tucker relations [15], [16] is ruled out. Also it is not guaranteed that the optimization problem is convex, such that a global optimization routine is preferred. For convergence issues an adaptive ES algorithm was chosen (c.f. Fig. 6) [17], [18]. For this case study the timing, peak laser power and FWC were picked as DOF. After defining the feasible domain of the DOF initial FOMs are evaluated and stored. According to the adaptive scheme of [17], [18] new offsprings (DOF) are generated in each iteration. Candidates that do not comply with the constraints are rejected. In this phase a certain amount of trials are made to generate feasible candidates. Subsequently the FOMs of those candidates are evaluated and compared to the former generation. The new generations are then composed of the best candidates from both generations. In this work 10 parents and 60 offsprings were chosen. Currently, the bottleneck of this algorithm is the rejection rate of candidates in the vicinity of the boundary constraints and the evaluation of the FOMs, which is not yet highly parallelized.

A MATLAB implementation proves the applicability of the proposed model in combination with the adaptive, global $(10 + 60)$-ES optimizer for the non-linear, constrained problem (Fig. 7). As saturation did not occur, the optimal FWC was low compared to a wider dynamic range application, provided no HDR scheme is applied. Calculation of the presented 100 iterations took 2.5 days.

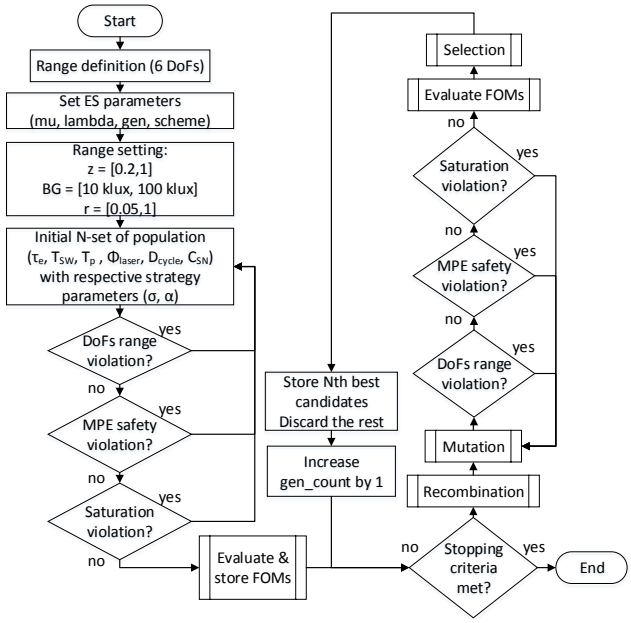

Figure 6. Program flow of adaptive (10+60)-ES optimizer with discrete and intermediate recombination and adaptive mutation of 10 parents and 60 offsprings.

In a brute force approach an optimization of these 6 DOF with a grid spanned by only 20 points per DOF would last 1.3 months if 100 evaluations could be performed per second. However, here it is to be taken into account that such a rough grid would hardly result in a global optima, proving that the presented algorithm indeed is significantly more efficient.

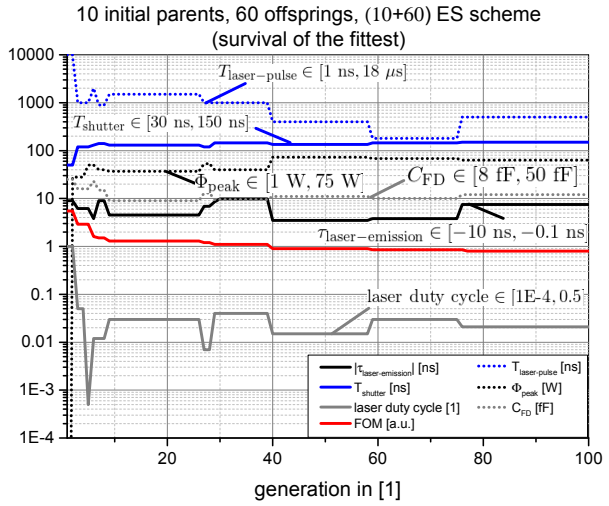

Figure 7. Simulation results from (10+60)-ES optimizer showing the candidate with best FOM after each iteration.

IV. Conclusion

The presented model offers a significantly faster computation of the precision of range imaging systems than before. This allows the user to employ dedicated global optimizers such as the presented ES algorithm to compute e.g. the optimal timing or HDR mode, which before was impractical. In the future optimization of HDR schemes will be investigated. It is desirable to derive a physical expression for the form of the kernel so that specifications can be translated to photodetector design more efficiently. The presented model is based on linearization which for large signal characteristics would result in an increased systematic error. Thus finding numerical algorithms for the approximation of the inverse function remains a challenge in PM iToF imaging.

References

[1] R. Lange, "3D Time-of-Flight Distance Measurement with Custom Solid-State Image Sensors in CMOS/CCD-Technology," Ph.D thesis, University of Siegen, 2012.

[2] K. Yasutomi et al., "A Time-Of-Flight Image Sensor with Sub-mm Resolution Using Draining Only Modulation Pixels," International Image Sensor Workshop 2013 , June. 2013.

[3] A. Payne et al., "A 512x424 CMOS 3D Time-of-Flight Image Sensor with Multiple-Frequency Photo-Demodulation up to 130MHz and 2GS/s ADC," IEEE International Solid-State Circuits Conference (ISSCC) 2014, pp. 134-136, Feb. 2014.

[4] T.Y. Lee et al., "A Time-of-Flight 3-D Image Sensor With Concentric-Photogates Demodulation Pixels," IEEE Transactions on Electron Devices, vol. 61, no.3, pp. 870-877, Mar. 2014.

[5] A. Süss et al., "Speed Considerations for LDPD Based Time-of-Flight CMOS 3D Image Sensors," European Solid State Circuits Conference (ESSCIRC), 2013, pp. 299-302, Sep. 2013.

[6] D. Stoppa et al., "Time Of Flight Image Sensors in 0.18 µm CMOS Technology: a Comparative Overview of Different Approaches," International Image Sensor Workshop 2011, June. 2011.

[7] R. Jeremias, "CMOS Bildsensoren mit Kurzzeitverschluß zur Tiefenerfassung nach dem Lichtlaufzeit-Meßprinzip," Ph.D thesis, University of Duisburg-Essen, 2009.

[8] M. Schmidt, "Analysis, Modeling and Dynamic Optimization of 3D Time-of-Flight Imaging Systems," Ph.D thesis, University of Heidelberg, 2011.

[9] A. Spivak et al., "Analysis of Gated CMOS Image Sensor for Spatial Filtering," IEEE Transactions on Electron Devices, vol. 60, no.1, pp. 305-313, Jan. 2013.

[10] A. Theuwissen, "Solid-State Imaging with Charge-Coupled Devices," 1st ed. Kluwer Academic Publishers, 1995.

[11] J.R. Janesick, "Scientific Charge-Coupled Devices," 1st ed. SPIE Press, 2001.

[12] A. Süss, "High Performance CMOS Range Imaging," Ph.D thesis, University of Duisburg-Essen, 2014.

[13] A. Spickermann et al., "Time-of-Flight Principle and Intrinsic Lateral Drift-Field Photodiode Pixels," European Solid State Circuits Conference (ESSCIRC), 2011, pp. 111-114, Aug. 2011.

[14] D. Durini et al., "Lateral drift-field photodiode for low noies, high-speed, large photo-active-area CMOS imaging applications," Nuclear Instruments and Methods in Physics Research Section A, 624, pp. 470-475, Dez. 2010.

[15] "IEC 60825-1 - Safety of Laser Products - Part 1: Equipment Classificaton," 1.2 ed, Aug. 2008.

[16] M. Papageorgiou et al., "Optimierung," 3rd ed. Springer, 2012.

[17] T. Bäck, "Evolutionary Algorithms in Theory and Practice," Oxford University Press, 1996.

[18] H..P. Schwefel, "Evolution and Optimum Seeking," 6th ed. Wiley, 1995.